Desalination and Water Treatment
www.deswater.com

doi:10.5004/dwt.2017.20936

82 (2017) 101–113
July

Magnetic $NiFe_2O_4$ decorated-exfoliated graphite for adsorptive removal of anionic dyes and cationic dyes from aqueous solution

Bui Thi Phuong Quynh[a,*], Sang Hoon Kim[b,*], Doan Thi Que Minh[c], Nguyen Thi Mong Diep[c], Pham Van Thinh[d], Nguyen Thi Thuong[a]

[a]*Faculty of Chemical Engineering, Ho Chi Minh City University of Food Industry, Ho Chi Minh City 705800, Vietnam, Tel. 84-8-38161673, Fax 84-8-3816-1673, email: phuongquynh102008@gmail.com, quynhbtp@cntp.edu.vn (B.T.P. Quynh)*
[b]*Center for Materials Architecturing, Korea Institute of Science and Technology, Seoul 136-791, Korea, Tel. 82-2-958-5426, Fax 82-2-958-5391, email: kim_sh@kist.re.kr (S.H. Kim)*
[c]*NTT Institute of Hi-Technology, Nguyen Tat Thanh University, Ho Chi Minh City 702000, Vietnam, Tel. 84-8-3940-5875, Fax 84-8-3940-4759, email: thuong.ngt88@gmail.com (N.T. Thuong), Mp.minh87@gmail.com (D.T.Q. Minh), nguyenthimongdiep05@gmail.com (N.T.M. Diep)*
[d]*Faculty of Food Technology, Environment and Nursing, Dong Nai University of Technology, Bien Hoa City 810000, Dong Nai, Tel. 84-61-3996-473, Fax 84-61-3996-915, email: phamvanthinh27@gmail.com (P.V. Thinh)*

Received 14 February 2017; Accepted 15 May 2017

ABSTRACT

This study focused on the fabrication, characterization of magnetic $NiFe_2O_4$-decorated exfoliated graphite (MEG) as well as its potential application as a low-cost, flexible and efficient adsorbent to remove different kinds of cationic and anionic dyes from aqueous solution. The exfoliated graphite was first fabricated using highly efficient microwave-assisted exfoliation technique and the ferrite magnetic component ($NiFe_2O_4$) was then introduced to the graphitic structure by sol-gel process. The materials were characterized using relevant analytical techniques such as scanning electron microscope (SEM), X-ray diffraction (XRD), Fourier transform infrared spectroscopy (FTIR), N_2 adsorption measurement and vibrating sample magnetometry. The adsorption behavior of widely used ionic dyes including methylene blue (MB), crystal violet (CV), methyl orange (MO) and congo red (CR) was investigated under effects of exfoliation degree, $NiFe_2O_4$ loading on EG structure, preparation temperature and adsorption conditions (i.e. pH and dye concentration). The adsorption mechanism was discussed taking into account the electrostatic force, hydrogen bonding, π–π interaction between delocalized π electrons of the basal planes and free electrons of aromatic rings and multiple bonds in dye molecules.

Keywords: Ionic dyes; Exfoliated graphite; Adsorption; Magnetic adsorbent; Nickel ferrite; Wastewater treatment

1. Introduction

Synthetic organic dyes are largely used in a variety of industrial activities such as papers, rubber, cosmetics, mills, printing, dyestuff, and food industries thus leading to the discharge of a huge amount of colored effluents to water bodies [1]. There are three groups of commonly used dyes, namely anionic (direct, acid and reactive) dyes, cationic (basic) dyes and non-ionic (vat and dispersed) dyes [2]. Many dyes and their degradation products are known to be highly toxic, non-biodegradable, carcinogenic and mutagenic [3,4]. Because of the persistency and toxicity of synthetic dyes, inadequate treatment of the dye contaminated wastewaters may result in deterioration of ecological balance and cause serious threats to aquatic life and human health [1,5]. Among a number of traditional and newly developed treatment methods, adsorption technology is still globally preferred in

*Corresponding authors.

decontamination of colored effluents owing to a number of advantages such as high efficiency, fast treatment process, absence of toxic by-products, simple design and operation of treatment infrastructure, applicability to large-scale systems and economic feasibility [3,6].

In adsorption technology, the last several decades have seen huge progress in development of adsorbents derived from numerous precursors ranging from naturally occurring to synthetic materials for sequestration of dyes from wastewaters, such as agricultural biomass, carbon-based substances, inorganic nanoparticles, inorganic-organic nanohybrids, and polymeric nanocomposites [7–10]. Among a myriad of materials, modified graphite/graphene based composites [11–15] have been found to possess high adsorption capacities for dye molecules owing to their superior properties such as light density, high surface area, abundance in oxygen-containing groups for coordinating with pollutant molecules [13,15]. An extensive survey of the literature revealed that the adsorption capacity and selectivity of graphite/graphene related adsorbents varied largely depending on the applied modification strategy. Various chemical means such as oxidation, intercalation using intercalants and/or several kinds of physical treatments such as thermal shock and ultra-sonication have been employed in attempts to develop pristine graphite into efficient adsorbents [13,15–18]. However, existing disadvantages of developed graphene based adsorbents including strong dependence of adsorption performance on environmental conditions such as pH value, complicated fabrication routes and thus relatively high fabrication cost [11,14,18–20] appear to limit their applicability, especially in harsh environment.

Exfoliated graphite (EG) is a kind of modified graphite; apart from graphene structure, it has incompleted separation between adjacent carbon layers and can be fabricated using low-cost, simple and easily reproducible techniques [21,22]. An expansion of tens to hundreds of times along c-axis could be achieved by applying chemical intercalation followed by microwave irradiation or rapid heating (thermal shock) [21–24]. Expanded graphite layers have a highly porous, worm-like structure, high surface area, light density and fascinating (mechanical, thermal, electrical, dielectric, adsorptive, etc.) properties beyond those of the pristine graphite, thus allowing numerous novel applications in fuel cells, electromagnetic interference shielding, vibration damping, and thermal interfacing [22,24–26]. Concerning with applications in environmental treatment, EG can be a promising cost-effective platform for adsorptive removal of pollutants owing to advantages such as cost-effectiveness, facile and reproducible fabrication routes, and expected good adsorption capacities for various pollutants.

The efficient collection of used adsorbents from aqueous solution to prevent material loss and to avoid pollution caused by residual adsorbents is important in practical applications. Recently, the magnetic phase separation has emerged as an ideal solution to address this problem [27–31]. Among many magnetic materials, the trevorite ($NiFe_2O_4$), an important AB_2O_4 spinel compound, has found numerous important applications in diverse areas ranging from ferrofluids, drug delivery, high-density information storage, electrocatalysis, gas sensors to biomedicine [32–34]. $NiFe_2O_4$ is a cubic ferromagnetic oxide with a typical inverse spinel structure where divalent Ni cations occupy the octahedric B sites and trivalent Fe cations equally locate between tetrahedric A-sites and octaheric B-sites [33,35]. The nanosized $NiFe_2O_4$ particles have been prepared by different methods such as sol-gel, solid-state reaction, co-precipitation, combustion, sonochemical and hydrothermal process [33,35]. When the use of magnetic oxide solely as adsorbent is still problematic due to costly fabrication process, slow adsorption rate and narrow working pH ranges [4,36], the development of composite of carbon materials and magnetic oxides, such as $NiFe_2O_4$, appeared as an ideal alternative. However, to our best knowledge, investigations on fabrication of exfoliated graphite-$NiFe_2O_4$ composite and its adsorption capacities for ionic dyes have not yet been conducted adequately.

In present study, a magnetic exfoliated graphite-$NiFe_2O_4$ composite was developed and its adsorption performance for the four common synthetic dyes, including methylene blue (MB), crystal violet (CV), methyl orange (MO) and congo red (CR) was investigated. To synthesize the magnetic adsorbent, the exfoliated graphite was first prepared from the natural graphite flakes via a simple two-step process of chemical intercalation using H_2SO_4/H_2O_2 and microwave-assisted expansion followed by magnetic decoration of $NiFe_2O_4$ via acid citric-based sol-gel process. Effects of synthesis process and adsorption conditions on adsorption behavior of the dyes were investigated. The characteristics of adsorbents were determined by scanning electron microscope (SEM), X-ray diffraction (XRD), Fourier transform infrared spectroscopy (FTIR), N_2 adsorption measurement and Vibrating sample magnetometry.

2. Experimental

2.1. Chemicals

All chemicals were used without any further purification. Synthetic dyes including methylene blue (MB), crystal violet (CV), methyl orange (MO) and congo red (CR) were purchased from HiMedia Laboratories Pvt. Ltd. Sodium hydroxide (NaOH), sulfuric acid (H_2SO_4 98%), hydrogen peroxide (H_2O_2, 30%) hydrochloric acid (HCl, 36%), ammonia solution (25%), citric acid ($C_6H_8O_7.H_2O$), nickel(II) chloride ($NiCl_2{\cdot}6H_2O$), and ferric chloride ($FeCl_3{\cdot}6H_2O$) were purchased from Xilong Chemical Co., Ltd. The Vietnamese natural graphite flakes (Yen Bai, Viet Nam) with an averaged granule size of about 1.25 mm and carbon content ≥ 90% were used as precursor.

2.2. Preparation of exfoliated graphite (EG)

The EG was synthesized by chemical intercalation process using H_2O_2 (30%) as oxidizing agent and H_2SO_4 (96%) as intercalating agent. In a typical intercalation process, the natural graphite flakes (G) were added into the mixture of H_2SO_4 and H_2O_2 (100:7 v/v). After 50 min, the intercalation mixture was continually washed with water until pH value reached 5–6. Then, the resulted black powder was collected by vacuum filtering and dried at 80°C for 24 h. The exfoliation was conducted in a microwave oven at the power of 750 W for 10 s.

The magnetic $NiFe_2O_4$-incorporated EG (MEG) was synthesized as follows. The aqueous solution of $NiCl_2{\cdot}6H_2O$ and $FeCl_3{\cdot}6H_2O$ (molar ratio of Ni^{2+}:Fe^{3+} as 1:2) were added into a beaker and stirred until obtaining complete dissolution of the metal salts. After that, the citric acid solution (molar ratio of $C_6H_8O_7$:Ni^{2+} as 12:1) and EG was subsequently added. The examined weight ratios between EG and $NiFe_2O_4$ in the composite were 85:15, 80:20 and 75:25. The EG samples loaded with 15 wt%, 20 wt%, 25 wt% of $NiFe_2O_4$ were labeled as MEG1, MEG2 and MEG 3, respectively. The pH of solution was increased to 9 by drop-wise adding ammonia solution to the mixture under vigorous stirring. Then, the temperature of solution was increased to 80°C until obtaining a viscous liquid which was further dried at 100°C in the oven for 2 d. The received dry powder was calcined in the temperature range of 200–800°C for 2 h to obtain the $NiFe_2O_4$-decorated EG samples.

2.3. Batch adsorption studies.

The adsorption behavior of four ionic dyes including crystal violet (CV), methylene blue (MB), methyl orange (MO), and congo red (CR) was studied under batch mode. The molecular structures and characteristics of the dyes are presented in Fig. 1 and Table 1 [7,37–40]. A predetermined amount of adsorbent was added into 100mL solution of a known dye concentration in a 250-mL Erlenmeyer flask. Preliminary tests showed that the dye adsorption on EG reached equilibrium after 30 min so the contact time of 30 min was applied for the adsorption tests. The effect of dye concentration was studied in the range of 20–200 mg/l with an MEG dosage of 3 g/l in neutral pH solution. Impact of pH value was observed in the 3–10 range at an MEG dosage of 3 g/l and initial dye concentration of 100 mg/l. The pH value was adjusted by either 0.1M HCl or 0.1 M NaOH. All adsorption experiments were performed at ambient temperature (30 ± 2°C) using an orbital shaker operating at 180 rpm.

The percentage removal of dye was determined by:

$$\textit{Removal efficiency}\ (\%) = \left(1 - \frac{C}{C_o}\right) \times 100\% \quad (1)$$

where C_o and C are the initial and residual dye concentration (mg/L) respectively.

The dye uptake at equilibrium per gram of adsorbent, q_e (mg/g) was calculated by:

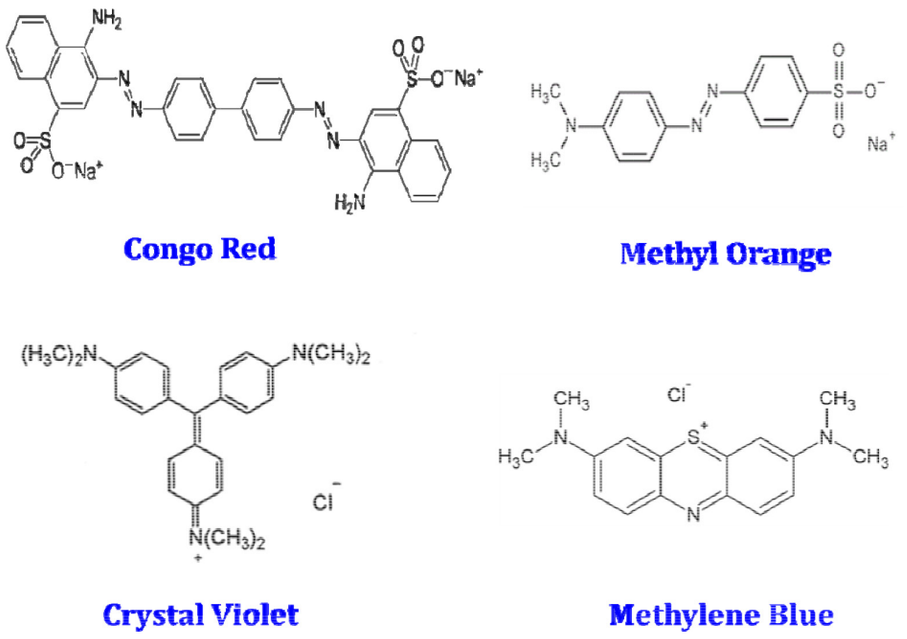

Fig. 1. Molecular structures of Congo Red, Methyl Orange, Crystal Violet and Methylene Blue.

Table 1
Characteristics of dye molecules and detection wavelengths

Type of dye	Molecular formula	Molecular weight (g/mol)	Molecular size	Wavelength (nm)	Reference
Methylene blue	$C_{16}H_{18}ClN_3S$	319.86	1.7 nm × 0.76 nm × 0.33 nm	664	[38]
Congo red	$C_{32}H_{22}N_6Na_2O_6S_2$	696.66	2.5 nm × 0.7 nm × 0.43 nm	500	[7,37,61]
Crystal violet	$C_{25}H_{30}ClN_3$	407.98	0.97 nm × 0.97 nm × 0.97 nm	583	[39]
Methyl orange	$C_{14}H_{14}N_3NaO_3S$	327.34	1.19 nm × 0.67 nm × 0.38 nm	463	[40]

$$q_e = \frac{\left(\left(C_o - C_e\right) \times V\right)}{m_a} \quad (2)$$

where C_o and C_e are the initial and equilibrium dye concentrations (mg/L), respectively; V is the volume of solution (L), and m_a is the adsorbent dosage (g/L).

2.4. Adsorption isotherm models

The construction of adsorption isotherms is important to understand the insights of adsorption process and to derive important parameters revealing possible reaction mechanisms. Among a number of isotherm models, Langmuir and Freundlich isotherms are commonly used to analyze the relationship between the concentration of adsorbate present in bulk solution and the amount adsorbed on adsorbent surface [41].

The Langmuir model is established assuming that the adsorption happens at homogeneous sites on the adsorbent surface and the saturated state is obtained when a monolayer of adsorbates is formed. The lateral interaction between the adsorbed molecules is considered negligible. The Langmuir isotherm model is expressed as follows [41,42]:

$$q_e = \frac{\left(K_L q_m C_e\right)}{\left(1 + K_L q_m C_e\right)} \quad (3)$$

This equation can be expressed in the linear form as:

$$\frac{1}{q_e} = \frac{1}{\left(K_L q_m C_e\right)} + \frac{1}{q_m} \quad (4)$$

where C_e (mg/L) and q_e (mg/g) are equilibrium concentration and adsorption capacity respectively; q_m (mg/g) and K_L (L/mg) are the maximum adsorption capacity and rate of adsorption, respectively.

The essential characteristics of Langmuir isotherm can be interpreted via the dimensionless equilibrium parameter (R_L) which is defined by [41,42]:

$$R_L = \frac{1}{\left(K_L C_o\right)} \quad (5)$$

where K_L (L/mg) is the Langmuir constant and C_o (mg/L) is the highest initial concentration. The type of adsorption isotherm is determined by the value range of R_L: unfavorable ($R_L > 1$), linear ($R_L = 1$), favorable ($0 < R_L < 1$) and irreversible ($R_L = 0$).

The Freundlich adsorption isotherm describes the adsorption behavior on the heterogeneous surface [11]. This model takes into account the mutual interaction between adsorbed molecules. The highly active sites should be occupied first and the affinity for binding will decrease upon the increasing occupation. The Freundlich model is described by the following equation [41]:

$$q_e = K_F \cdot C_e^{\frac{1}{n}} \quad (6)$$

The equation can be rearranged into the linear form as:

$$lnq_e = lnK_F + \frac{1}{n} lnC_e \quad (7)$$

where $1/n$ and K_F [(mg/g)·(L/mg)$^{1/n}$] are Freundlich constants related to the favorability of adsorption process and the adsorption capacity of the adsorbent, respectively. The heterogeneity factor, $1/n$, expresses adsorption intensity of adsorbent; the adsorption bond is stronger with decreasing $1/n$ value.

2.5. Characterization methods

The dye concentration was determined by measuring the absorbance at a constant wavelength for each kind of dye (664 nm for MB, 583 nm for CV, 500 nm for CR, 463 nm for MO) using an Evolution 60S UV-Visible spectrophotometer (Thermo Fisher Scientific, USA). The calibration curves were constructed by plotting the absorbance of each single dye against dye concentration at a fixed wavelength.

The scanning electron microscope (SEM) analysis was performed on a S4800 instrument (Japan). The X–ray powder diffraction (XRD) measurement was implemented on a D8 Advance Bruker powder diffractometer with a Cu–K_α excitation source. The diffraction spectra were recorded with a scan rate of 0.02°/s in the 2-theta range of 2–90°. The textural properties of the adsorbents were determined by N_2 adsorption/desorption measurement at 77 K in a Micromeritics 2020 analyzer. Specific surface area was determined using Brunauer–Emmett–Teller (BET) equation. The FTIR spectra were recorded in the range of 4000–400 cm^{-1} using a Bruker ALPHA FT-IR (Fourier transform infrared) spectrophotometer using KBr as a matrix. Measurement of static magnetic moment was conducted on a GMW 3474-140 magnetometer equipped with a superconducting magnet to produce the fields up to 16 KOe.

3. Results and discussion

3.1. Preparation of exfoliated graphite (EG) for dye adsorption

The influence of preparation conditions on adsorption capacity of the EG was first investigated. The EG was synthesized by microwave-assisted exfoliation of the graphite intercalated compounds (GICs) which were prepared by chemical intercalation involving H_2O_2 (30%) as oxidizing agent and H_2SO_4 (96%) as intercalating agent [21]. In an effort to obtain well-expanded graphite structure with good adsorption performance, different volume ratios of H_2SO_4:H_2O_2:G were investigated. The prepared EG samples were applied for the adsorption of a cationic dye, crystal violet (CV), and an anionic dye, methyl orange (MO). The amount of natural graphite flakes was fixed at 1g (1.6 cm^3) for all experiments while varying the volume of H_2SO_4 and H_2O_2 solution. The batch adsorption studies were carried out using a MEG dosage of 3 g/l and an initial dye concentration of 100 mg/l in neutral aqueous solution. The bulk density, ratio of bulk density of EG and G (graphite) and dye removal efficiencies of the representative EG samples are presented in Table 2**.** It was found that the expansion volume of EG samples depended significantly on H_2SO_4/H_2O_2/G volume ratio and correlated well with the corresponding dye removal efficiencies. The EG2 (H_2SO_4:H_2O_2:G ratio of 12.5:1:1) exhibited the largest expansion degree (d_G/

Table 2
Effect of intercalation conditions on expansion degree and dye removal efficiency of exfoliated graphite samples

Sample	Volume ratio of H_2SO_4: H_2O_2:G_{bulk} (*)	d_{EG} (10^{-3}·g/cm^3)	d_G/d_{EG}	%CV removal	%MO removal
EG1	6.25:1:1	10.2	62.07	51.96	25.71
EG2	12.5:1:1	5.6	113.05	84.87	66.32
EG3	12.5:1.875:1	8.4	75.37	61.57	39.33
EG4	15:1:1	7.6	83.30	78.01	63.75

(*)The mass of natural graphite flakes was fixed at 1 g, equivalent to 1.6 cm^3 of bulk volume (with d_G = 0.625 g/cm^3).

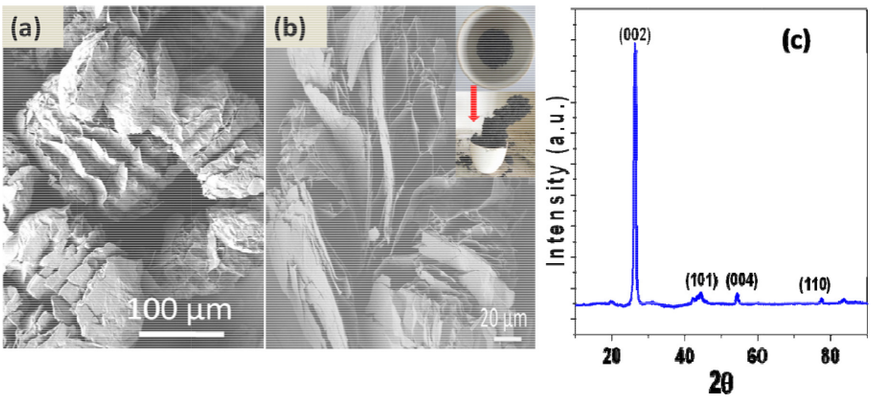

Fig. 2. Characterization results of the exfoliated graphite (EG2): SEM images (a&b) and XRD pattern (c).

d_{EG} of 113) and also highest removal percentages for both CV (84.87 %) and MO (66.32%). Note that the pristine natural graphite flakes exhibited inconsiderable adsorption capacity as compared to the exfoliated ones so the result is not presented here. Further increase in volume fraction of both H_2SO_4 and H_2O_2 resulted in decrease of adsorption capacity; however, the excessive amount of H_2O_2 led to more negative effect in intercalation process which is in good agreement with the previous study [21]. In good accordance with expectation, the SEM image of EG2 reveals a highly porous worm-like structure (Fig. 2a) composed of significantly expanded graphite layers and a large amount of macroporous interconnected pores (Fig. 2b). The surface of graphite walls appeared to be highly rough and rich in defects which are expectedly active in adsorption process. Moreover, the XRD pattern of EG2 (Fig. 2c) shows the presence of (002) graphite plane at 2θ = 26.5° with the absence of peaks of oxidized species indicating that the graphitic nature was still maintained after exfoliation [43]. Based on the above results, the volume ratio of H_2SO_4:H_2O_2: G as 12.5:1:1 (EG2) was selected to prepare the exfoliated graphite for further investigations.

3.2. Magnetic $NiFe_2O_4$-decorated exfoliated graphite (MEG) for adsorption of cationic and anionic dyes

3.2.1. Characteristics of MEG

The magnetic adsorbents composed of EG and $NiFe_2O_4$ species were prepared via sol-gel process followed by drying and calcination at elevated temperatures. The synthesis conditions were first optimized for the sake of obtaining the magnetic composite with sufficient susceptibility to magnetic field for efficient phase separation. The magnetic behavior of the MEG samples was evaluated via magnetic hysteresis loops (M–H curves) which were obtained by recording magnetization against applied magnetic field at room temperature using a vibrating sample magnetometer (VSM). Fig. 3a shows the influence of fabrication temperature on the magnetic property of the MEG with 20wt% $NiFe_2O_4$. The magnetization value of the EG-20wt%$NiFe_2O_4$ prepared at 200°C and 400°C could not approach a saturation level (the inset in Fig. 3a) but further increase in fabrication temperature to 600°C led to a well-defined saturation magnetization Ms at 11.8 emu/g. The Ms value went up to 21 emu/g as the temperature increased to 800°C which was related to the growth of $NiFe_2O_4$ particle size [33]. The influence of $NiFe_2O_4$ content on the M–H curves can be observed in Fig. 3b. The EG samples loaded with 15 wt%, 20 wt%, 25 wt% $NiFe_2O_4$ were labeled as MEG1, MEG2 and MEG3 respectively; the calcination temperature of all samples were fixed at 600°C. It can be seen that the hysteresis loops of all samples show the characteristics of ferromagnetic materials. The Ms value increased gradually from 6.9 to 14.2 emu/g when the $NiFe_2O_4$ content increased from 15 wt% to 25 wt%. Under current experimental conditions, the $NiFe_2O_4$ loading of 20 wt% with the Ms value of 11.8 emu/g was at least required for efficient magnetic phase separation in water and dye solution under an external magnetic field as illustrated in Fig. 4. The XRD patterns of MEG samples (Fig. 5) contain the peaks of $NiFe_2O_4$ crystalline phase in

addition to the diffraction peaks of graphitic structure, for example the peaks at 35.66°, 42.41° and 62.93° corresponding to (331), (400) and (440) planes of $NiFe_2O_4$ respectively [44,45], revealing the successful formation of $NiFe_2O_4$ phase incorporated into exfoliated graphite structure. As the $NiFe_2O_4$ concentration increased, the intensities of their corresponding crystalline peaks were also increased.

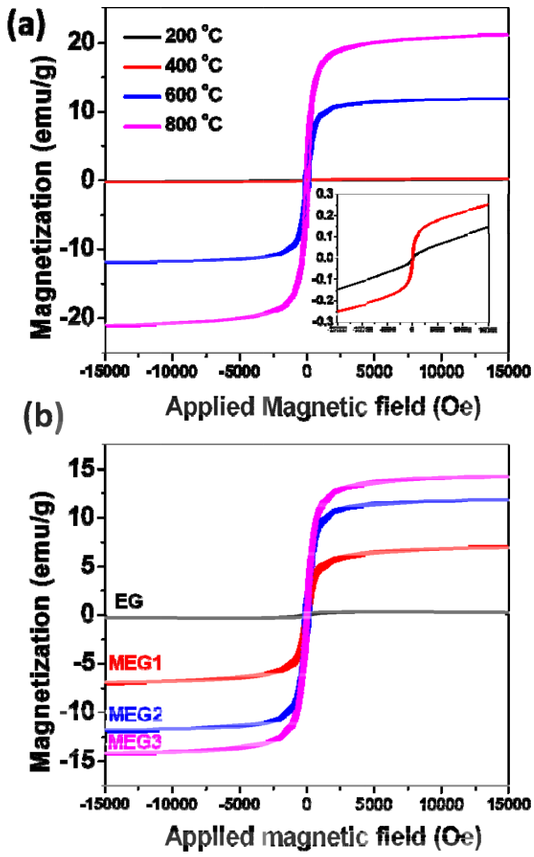

Fig. 3. M–H curves for exfoliated graphite based adsorbents: (a) effect of calcination temperature observed on MEG2 and (b) effect of $NiFe_2O_4$ content. The inset in Fig. 3a represents M–H curves of the MEG samples prepared at 200°C (black) and and 400°C (red).

The change in textural properties of the graphite upon modification was determined via N_2 adsorption measurement. The analysis results of EG-20wt%$NiFe_2O_4$, EG and G are provided in Fig. 6 and Table 3. The BET surface area, external surface area and pore volume (supermicro-meso pores) estimated from t-Plot and mesopore size (1.7 nm –300 nm) distribution of graphite obtained from BJH analysis are shown in Fig. 6 and Table 3. The application of microwave-assisted exfoliation supported nearly 10-fold increase of the BET surface area (total surface area), about 35-fold increase of the external surface, and 5-fold increase of micropore area. The external surface area here refers to the sum of area of the pore walls and outer surface of the expanded graphite flakes [46]. According to Fig. 6, as compared to the pristine graphite, the mesopore networks with a wide range of mesopore sizes were emerged owing to exfoliation process and the volume of 150–600 A° pores contributed mainly to the total mesopore volume. As a result, the cumulative pore volume (BJH) increased by more than 7 fold. Upon decoration of magnetic $NiFe_2O_4$, density of pores in size range of 100–650 A° increased but that of smaller pores (20–50 nm) decreased significantly. Accordingly, the BJH pore volume increased by 1.3 fold. Additionally, the external surface area reduced but the pore area increased remarkably based on t-Plot analysis. It may indicate that the $NiFe_2O_4$ nanoparticles blocked the pores in the

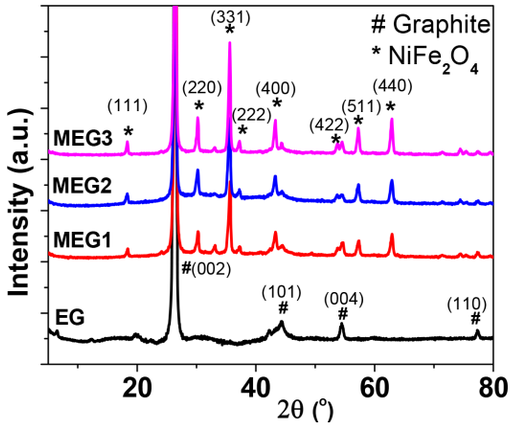

Fig. 5. XRD patterns of the MEG samples.

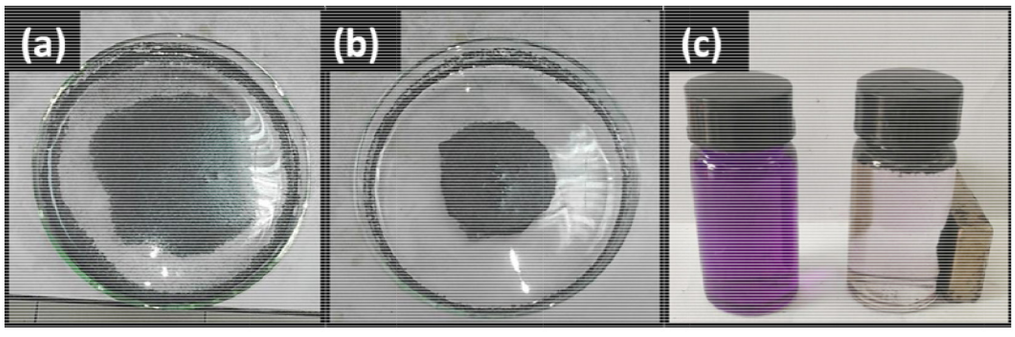

Fig. 4. Photos revealing the magnetic separation of the MEG adsorbents from aqueous solution using a magnet; (a) MEG1, (b) MEG2 in water and (c) MEG2 in CV dye solution.

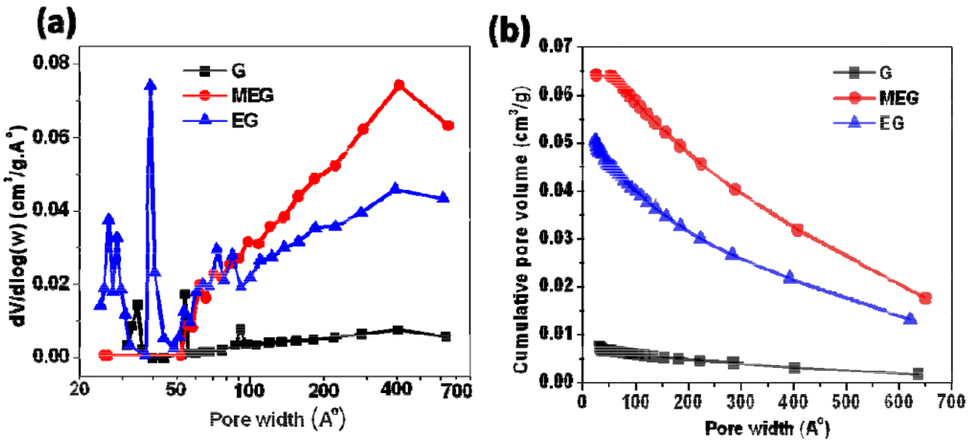

Fig. 6. Porosity analysis results of the graphite base adsorbents including graphite (G), exfoliated graphite (EG) and 20 wt% $NiFe_2O_4$ loaded exfoliated graphite (MEG): (a) BJH pore size distribution and (b) cumulative pore volume versus pore width.

Table 3
Textural properties of the graphite based adsorbents

Adsorbent	BET surface area (m^2/g)	t-Plot micropore area (m^2/g)	t-Plot external surface area (m^2/g)	t-Plot pore volume (cm^3/g)	BJH desorption cumulative pore volume (cm^3/g)(17-3000 A°)
Graphite flakes	3.1348	2.7043	0.4305	$1.037.10^{-3}$	$7.181.10^{-3}$
Exfoliated graphite (EG)	28.9720	14.0067	14.9653	$5.380.10^{-3}$	$50.478.10^{-3}$
EG-20wt% $NiFe_2O_4$	32.8708	25.9100	6.9608	$9.688.\ 10^{-3}$	$63.977.10^{-3}$

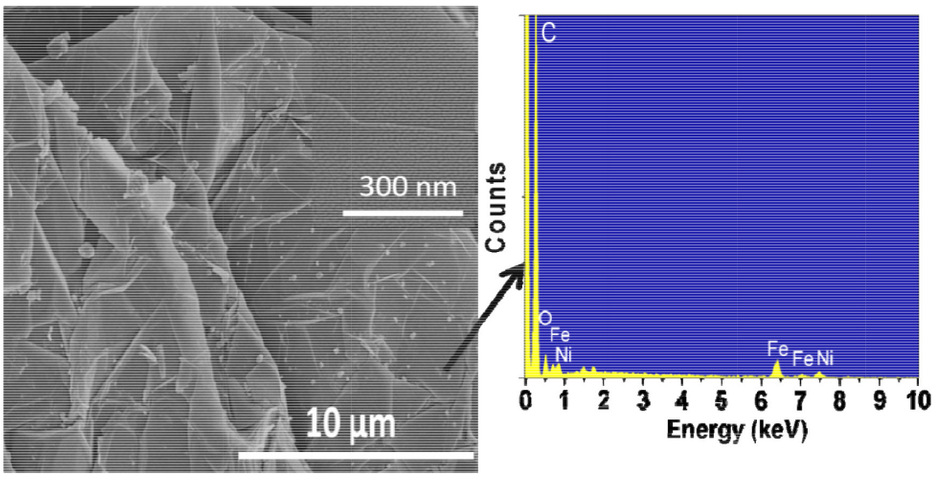

Fig. 7. SEM-EDS analysis of the MEG2.

20–50 nm range while the heat treatment at 600°C induced the widening of the existing pores and/or formation of new mesopore and micropore networks due to the leaving of gasified compounds. The even distribution of $NiFe_2O_4$ nanoparticles on graphite flakes of MEG2 sample in the large scale was observed using SEM analysis (Fig. 7). Moreover, the EDS spectrum shows the existence of C, O, Fe, Ni elements; the average weight concentrations of C, O, Fe and Ni were 74.56%, 11.66%, 8.48% and 4.47% respectively. In accordance with expectation, the total weight percent of Ni, Fe and O species was close to 20 wt% and the derived Fe/Ni atomic ratio approached 2.

3.2.2. *Adsorption behavior of cationic and anionic dyes on MEG*

Fig. 8 shows the percentage removal of CV and MB as cationic dyes, and MO and CR as anionic dyes using

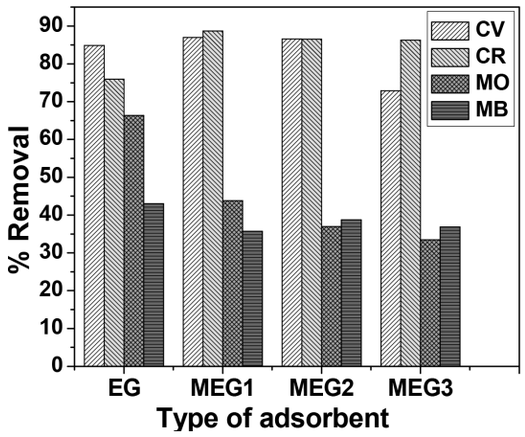

Fig. 8. Effect of $NiFe_2O_4$ content on dye removal efficiencies of the MEG adsorbents.

EG and MEG adsorbents consisting of different amounts of magnetic $NiFe_2O_4$ component. To study the effect of $NiFe_2O_4$ amount, the calcination temperature of all samples were fixed at 600°C. As it can be seen, the percentage removal of CR using MEG adsorbents was higher than with EG (ca. 86% vs. 76%); the treatment efficiency for CR did not change significantly upon variation of $NiFe_2O_4$ amount in the concentration range of 15–25wt%. The MEG adsorbents also exhibited high adsorption capacity for CV with about 87% decolorization obtained with MEG1 and MEG2; however the MEG3 provided only 72% removal which was even lower than EG revealing that the $NiFe_2O_4$ loading above 20 wt% started creating negative effect on the adsorption of CV. On the other hand, the adsorption of MO decreased from about 66% to 33% when increasing $NiFe_2O_4$ content from 15 to 25 wt%. Regarding MB, the percentage removal was in the range of 36–43% and the effect of $NiFe_2O_4$ was not clearly observed but MEG adsorbents showed lower removal efficiency than EG. In addition, it should be noted that although increasing calcination temperature enhanced the saturation magnetization of MEG but simultaneously reduced its adsorption capacities for the dyes (results are not shown here). In general, it can be concluded that the EG-20 wt% $NiFe_2O_4$ prepared at 600°C (MEG2) is the appropriate adsorbent which possesses not only sufficient magnetic property but also good adsorption capacities for different kinds of ionic dyes.

From the practical point of view, the contaminated effluents discharged from industrial activities normally have a strong variation in dye concentration and pH value. The pH of solution can have a profound impact on the adsorbent surface charge, dissociation of functional groups residing on the adsorbent surface and ionization degree of the adsorbates thus leading to changes in adsorption behavior [1,47]. Therefore, the effect of initial dye concentration in the range of 20–200 mg/l (Fig. 9a) and pH range of 3–10 (Fig. 9b) on decolorization efficiencies of MEG2 were investigated in the scope of this study. For MO and MB, there was a decrease trend in percentage removal when increasing dye concentration; the treatment efficiency was approximately 97% at 20 mg/l and then dropped severely to just around 20 wt% as the dye concentration increased to 200 mg/l. The percentage removal of CV was obtained at around 97% with the CV concentration below 50 mg/l followed by a significant decrease to 49% at 200 mg/l. In a different manner, the percentage removal of CR registered at ca. 78% at 20 mg/l and fluctuated around 87–89% in the concentration range of 50–200 mg/l.

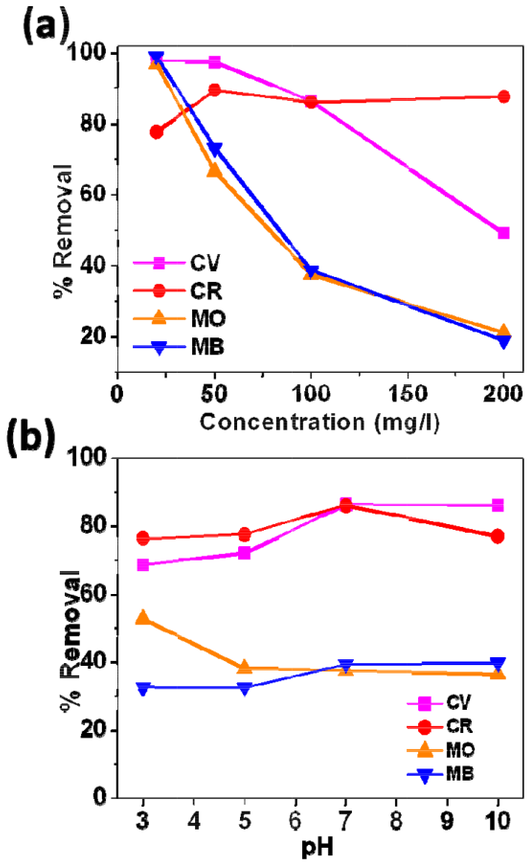

Fig. 9. Effect of initial concentration (a) and pH of solution (b) on dye removal efficiencies using MEG2 as adsorbent.

According to Fig. 9b which shows the impact of pH of solution on decolorization efficiency, the optimal pH value for eliminating CV, MB and CR was found to be around neutral value (pH = 7), with 86.18%, 86.45%, 39.32% removal achieved for CR, CV and MB respectively. It can be seen that MEG2 tent to remove CV and MB more efficiently as the solution became more basic. By contrast, the adsorption of MO appeared to be more favored in acidic solution with about 10% higher than in neutral and basic media. It can be explained that the excessive H^+ ions in acidic medium could compete with the cations to occupy the active carbon sites [48], thus possibly hindering the adsorption of CV and MB but promoting that of MO. On the contrary, a reverse phenomenon occurred in basic solution in which the competitive adsorption of excessive OH^- species could become a barrier for the adsorption of MO but likely enhanced the uptake of CV and MB [48]. It should be mentioned that the treatment efficiencies for these four dyes did not fluctuate widely in the pH range of 5–10. Such less susceptibility to pH of solution in this relatively wide pH range is suggested

to be an advantageous property of the as-prepared MEG as compared to other developed graphite/graphene based adsorbents [20] for prospective practical applications.

The study of adsorption isotherms with MEG2 adsorbent shows that the adsorption behavior of MO and CV were best consistent with the Langmuir model (Fig. 10a, Table 4), indicating the formation of monolayer coverage of the CV and MO molecules on the MEG surface. The fitting to the Langmuir model yielded maximum adsorption capacities of 35.97 mg CV/g and 16.03 mg MO/g with high correlation coefficients (R^2 of 0.9887 for CV and R^2 of 0.9772 for MO). The calculated R_L values of CV and MO are 0.0494 and 0.6459 respectively corresponding to favorable adsorption processes. The adsorption of MB appeared to obey relatively Langmuir model (R^2 of 0.9563) but the fitting to Freundlich isotherm model gave a higher R^2 value of 0.9784 (Fig. 10b). In the moderate concentration range of 20–100 mg/l, the adsorption of CR on MEG2 was favorable and followed well the Langmuir model as evidenced by R_L value of 0.2264 and R^2 value of 0.9971; however, a large deviation was observed at higher CR concentration (Fig. 10c). The maxium adsorption capacity as determined by Langmuir equation followed the order: 79.94 mg/g for congo red > 35.97 mg/g for crystal violet > 16.03 mg/g for methyl orange > 13.66 mg/g for methylene blue. Based on the above results, the EG-$NiFe_2O_4$ hybrid adsorbent, which is synthesized using facile and highly reproducible processes, can be a flexible and efficient platform for the treatment of wastewaters contaminated by cationic and anionic dyes.

3.2.3. Possible interactions between MEG and dye molecules

In attempts to find out possible chemical interactions between dye molecules and the MEG surface, FTIR analysis of the samples before and after adsorption was performed as shown in Fig. 11. The analysis of EG surface was also conducted for comparison. The spectrum of the as-prepared EG reveals presence of C–O stretching (1049 cm^{-1}), C–H asymmetric stretching (the broad band at 2931 cm^{-1} and 1380 cm^{-1}), deformation vibrations of adsorbed water and hydroxyl groups (3441 cm^{-1}), aliphatic C=C and C=O stretching (1631–1724 cm^{-1}), =C-H bending (667–759 cm^{-1}) [49,50]. Moreover, a small band characteristic of stretching vibration of gaseous CO_2 was also detected at 2356 cm^{-1} [51]. Upon incorporation of $NiFe_2O_4$ particles, the appearance of two adsorption bands peaking at around 597 cm^{-1} and 420 cm^{-1} is attributable to the stretching vibration of Fe^{3+}–O^{2-} in tetrahedral sites and that of bending vibrations in octahedral sites respectively [52,53]; the intensities of the bands for C–O and C=O stretching were reduced significantly but the new absorption peak (1539 cm^{-1}) emerged in this region. Additionally, the emergence of high frequencies hydroxyls at 3754 cm^{-1} can be related to the hydroxyls bonded to the crystalline Ni or Fe [54]. After adsorption of dyes, the band of C–H stretching was divided into two distinguishable bands peaking at ca. 2925 cm^{-1} and ca. 2850 cm^{-1} revealing the presence of long chain of $–CH_2$ groups [55]; additionally adsorption bands appeared more complicated in the region of 1280–1539 cm^{-1}, indicating the possible change in C–H bending or C=C stretching vibration [56,57]. Such changes were likely caused by the π–π interaction between electrons

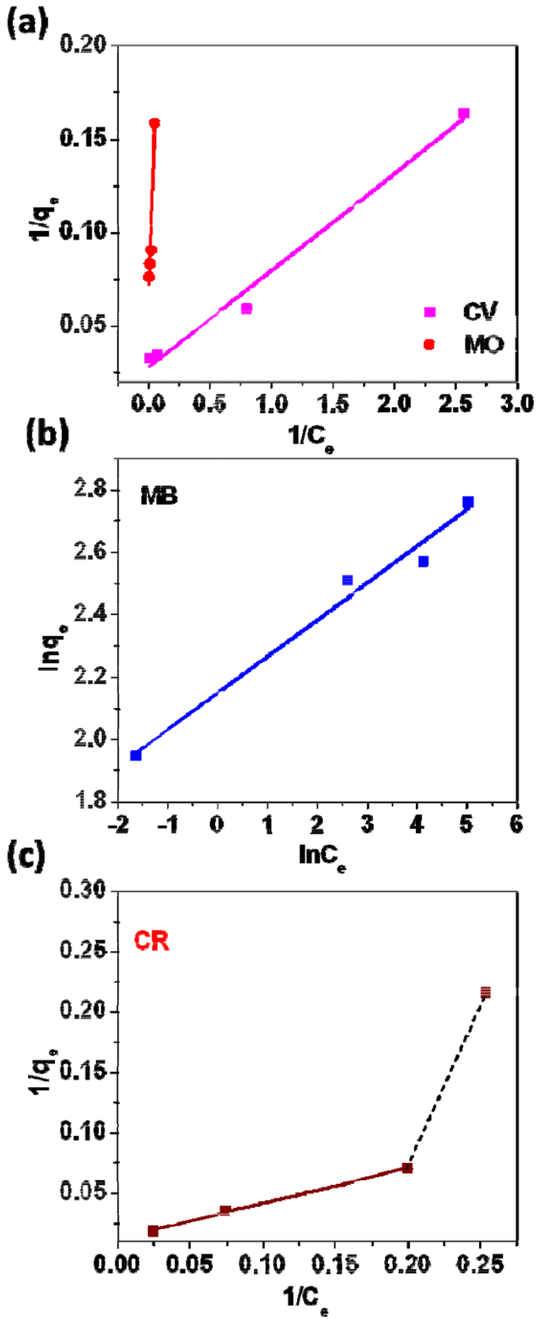

Fig. 10. Adsorption isotherms for adsorption of dyes on the MEG2.

of graphite layers and dye molecules. It is important to note that the absorption region of 540–574 cm^{-1} seemed to disappear upon the attachment of CV and CR, but not for MO and MB, demonstrating the formation of bonds between $NiFe_2O_4$ particles and CV and CR molecules.

For the two cationic dyes, MV and MB, the positive charge (+1) can be generated due to the withdrawal of lone pair of electrons on the sulfur (S) atom of MB and on the nitrogen atom of CV to the benzene ring. Regarding

Table 4
Adsorption isotherm parameters for dye adsorption on MEG

Dye	Langmuir isotherm model				Freundlich isotherm model		
	q_m (mg/g)	K_L (L/mg)	R_L	R^2	K_F [(mg/g)·(L/mg)$^{1/n}$]	$1/n$	R^2
CV	35.97	0.5346	0.0494	0.9887	11.2582	0.2701	0.7845
CR	79.94	0.0427	0.2264	0.9971	2.1582	0.9048	0.8549
MO	16.03*	0.0342*	0.6459*	0.9772*	2.7229	0.3177	0.8630
MB	13.66	0.0765	0.4888	0.9563	8.5840	0.1178	0.9784

*The Langmuir isotherm parameters derived in the concentration range of 20–100 mg/l for CR.

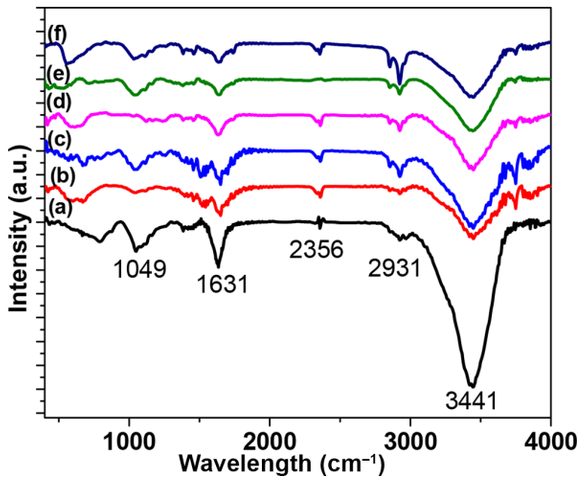

Fig. 11. FTIR analysis of the EG adsorbents: as-prepared EG (a); as-prepared MEG2 (b); MEG2 loaded with MV (c), MB (d), CR (e), MO (f).

the cationic dyes, beside the negatively charged sulfonic groups (SO_3^-), MO and CR molecules also contain other active functional groups such as azo groups (MO, CR) and amine groups (CR). Basically, the adsorption of ionic dyes on the MEG surface could be inspired by the following driving forces: (i) electrostatic forces induced by charges resided on MEG and oppositely charged functional groups of dye molecules, (ii) π-π interactions between delocalized π electrons of the basal planes of EG and free electrons of aromatic rings and multiple bonds in dye molecules, (iii) formation of hydrogen bonds between S, O, N atoms of dye molecules and the OH^- groups available on MEG, (iv) Van der Waals forces resulted from the interaction between permanent and/or instantaneously induced dipoles [1,15,58–60]. It should be noted that the Van-der Waal interaction is supposed to be important on planar surfaces rather than at edge and defect sites [60], thus this induced attractive force could possibly take a considerable part in dye adsorption on the planar EG surface and internal surface of interconnected network of macropores as well.

Despite the same static charge (+1) of the inonized CV and MB, MEG exhibited much higher removal efficiency for CV, indicating electrostatic interaction was not solely the mechanism of adsorption process. Both electrostatic interaction and π–π stacking may play essential roles in the adsorption process [15,39]. It is worth noting that adsorption of MB on MEG is much less favored than on other developed graphene related materials in which the electrostatic forces played the decisive role in adsorption mechanism [20]. In this case, the adsorption of MV and CR could occur on both EG structure and $NiFe_2O_4$ species as suggested by FTIR analysis; this is consistent with the above results which show the positive effect of $NiFe_2O_4$ on the removal efficiency for MV (up to 20 wt% $NiFe_2O_4$) and for CR (up to 25 wt% $NiFe_2O_4$). To some extent, the low adsorption efficiency for MB could be contributed partly by the adsorbate-adsorbate steric effect [39]. As the active sites (S atoms) for bonding located in the center of the linear MB molecules while N atoms located on vertex angles of the triangle structure of CV molecules, the expected linear configuration of MB when adsorbed on the graphite layer could block the adjacent active sites for the other adsorbates (Fig. 12a) while the CV molecules could possibly build up more efficiently over the carbon layer as benefited from the triangle configuration (Fig. 12b). On the other hand, the π–π dispersion interactions (Fig. 12c) and formation of hydrogen bonds between S, O, N atoms of dye molecules and functional groups on MEG are suggested to contribute mainly to the adsorption of anionic dyes like MO and CR. The more efficient adsorption of CR on MEG, as compared to MO, may benefit from the richer aromatic rings and more functional groups in the CR molecule structure and additional contribution of $NiFe_2O_4$ particles as indicated by the FTIR analysis.

4. Conclusions

The porous magnetic adsorbent developed by combining worm-like expanded graphite flakes and $NiFe_2O_4$ was demonstrated to be capable of sequestering efficiently and rapidly the common ionic dyes including methylene blue (MB), crystal violet (CV), methyl orange (MO) and congo red (CR), from the aqueous solution. The exfoliated graphite could be sufficiently magnetized with 20wt% $NiFe_2O_4$ to allow easy phase separation under external magnetic field without considerable compensation of adsorption performance. Among the four dyes, the EG-20wt%$NiFe_2O_4$ exhibited highest removal efficiencies for CV and CR. The presence of $NiFe_2O_4$ phase appeared to promote the adsorption of CV and CR but reduced the affinity towards MO and MB. The adsorption behavior of dye molecules was significantly affected by the initial dye concentration

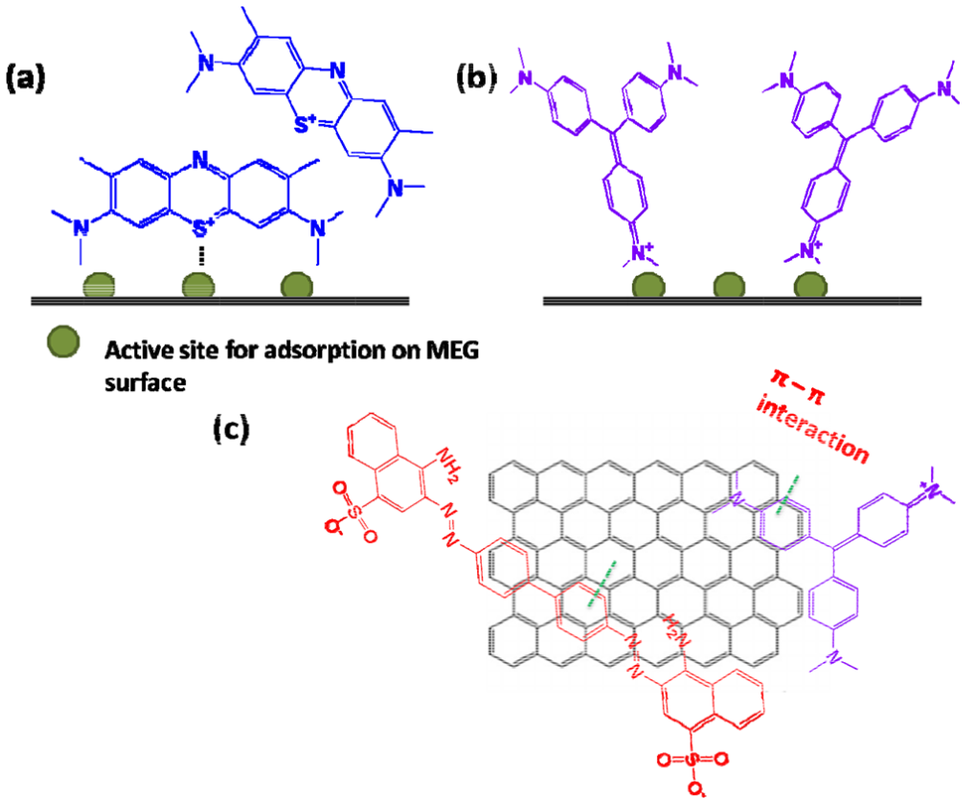

Fig. 12. Graphical illustration of possible interaction between the dyes and MEG surface; expected adsorbed MB(a) and CV(b) configuration, (c) possible π–π interactions between CV, CR and EG structure.

but a slight effect of variation in pH solution (5–10) was observed. The maximum adsorption capacity as determined by Langmuir equation followed the order: 79.94 mg/g for CR > 35.97mg/g for CV > 16.02 mg/g for MO > 13.66 mg/g for MB. According to the results of this study, the as-prepared magnetic exfoliated graphite with important advantages such as cheap precursor, facile and reproducible fabrication procedure, significant adsorption capacities for different kinds of dyes and low vulnerability to pH variation appears as a very promising platform for practical treatment of colored effluents.

Acknowledgement

This work was supported by a grant from the Korea Institute of Science and Technology (KIST) Institutional Program (Project No. 2Z04820-16-090), by a grant from the future R&D Program (2E26120) of the Korea Institute of Science and Technology (KIST), and by Foundation for Science and Technology Development from Nguyen Tat Thanh University, Ho Chi Minh City, Viet Nam.

References

[1] M.T. Yagub, T.K. Sen, S. Afroze, H.M. Ang, Dye and its removal from aqueous solution by adsorption: A review, Adv. Colloid. Interface Sci., 209 (2014) 172–184.

[2] K.B. Tan, M. Vakili, B.A. Horri, P.E. Poh, A.Z. Abdullah, B. Salamatinia, Adsorption of dyes by nanomaterials: Recent developments and adsorption mechanisms, Sep. Purif. Technol., 150 (2015) 229–42.

[3] Y. Li, W. Nie, P. Chen, Y. Zhou, Preparation and characterization of sulfonated poly(styrene-alt-maleic anhydride) and its selective removal of cationic dyes, Colloids Surf. A, 499 (2016) 46–53.

[4] L. Lu, J. Li, J. Yu, P. Song, H.L.N. Dickon, A hierarchically porous $MgFe_2O_4/\gamma$-Fe_2O_3 magnetic microspheres for efficient removals of dye and pharmaceutical from water, Chem. Eng. J., 283 (2016) 524–534.

[5] V.S. Munagapati, D.S. Kim, Adsorption of anionic azo dye congo red from aqueous solution by cationic modified orange peel powder, J. Mol. Liq., 220 (2016) 540–548.

[6] L. Yan, L. Qin, H. Yu, S. Li, R. Shan, B. Du, Adsorption of acid dyes from aqueous solution by CTMAB modified bentonite: Kinetic and isotherm modeling, J. Mol. Liq., 211 (2015) 1074–1081.

[7] L. Wang, A. Wanga, Adsorption behaviors of congo red on the N,O-carboxymethyl-chitosan/montmorillonite nanocomposite, Chem. Eng. J., 143 (2008) 43–50.

[8] M.J. Puchana-Rosero, M.A. Adebayo, E.C. Lima, F.M. Machado, P.S. Thue, J.C.P. Vaghetti, C.S. Umpierres, M. Gutterres, Microwave-assisted activated carbon obtained from the sludge of tannery-treatment effluent plant for removal of leather dyes, Colloids Surf. A, 504 (2016) 105–115.

[9] D.A. Giannakoudakis, G.Z. Kyzas, A. Avranas, N.K. Lazaridis, Multi-parametric adsorption effects of the reactive dye removal with commercial activated carbons, J. Mol. Liq., 213 (2016) 381–389.

[10] D. Robati, B.Mirza, R. Ghazisaeidi, M. Rajabi, O.Moradi, I. Tyagi, S. Agarwal, V.K. Gupta, Adsorption behavior of methylene blue dye on nanocomposite multi-walled carbon nanotube functionalized thiol (MWCNT-SH) as new adsorbent, J. Mol. Liq., 216 (2016) 830–835.

[11] Z. Xue, S. Zhao, Z. Zhao, P. Li, J. Gao, Thermodynamics of dye adsorption on electrochemically exfoliated graphene, J. Mater. Sci., 51 (2016) 4928–4941.
[12] Z.L. Xie, X. Huang, M.M. Titiricic, A. Taubert, Mesoporous graphite nanoflakes via ionothermal carbonization of fructose and their use in dye removal, RSC Adv., 4 (2014) 37423–37430.
[13] H. Yan, X. Tao, Z. Yang, K. Li, H. Yang, A. Li, R. Cheng, Effects of the oxidation degree of graphene oxide on the adsorption of methylene blue, J. Hazard. Mater., 268 (2014) 191–198.
[14] N. Zeinali, M. Ghaedi, G. Shafi, Competitive adsorption of methylene blue and brilliant green onto graphite oxide nano particle following: Derivative spectrophotometric and principal component-artificial neural network model methods for their simultaneous determination, J. Ind. Eng. Chem., 20 (2014) 3550–3558.
[15] F. Liu, S. Chung, G. Oh, T.S. Seo, Three-dimensional graphene oxide nanostructure for fast and efficient water-soluble dye removal, ACS Appl Mater Interfaces, 4 (2012) 922–927.
[16] M. Zhao, P. Liu, Adsorption of methylene blue from aqueous solutions by modified expanded graphite powder, Desalination, 249 (2009) 331–336.
[17] P. Bradder, S.K. Ling, S. Wang, S. Liu, Dye adsorption on layered graphite oxide, J. Chem. Eng. Data, 56 (2011) 138–141.
[18] M.N. Carvallho, K.S.D. Silva, D.C.S. Sales, E.M.P.L. Freire, M.A.M. Sobrinho, M.G. Ghislandi, Dye removal from textile industrial effluents by adsorption on exfoliated graphite nanoplatelets: kinetic and equilibrium studies, Water Sci. Technol., 73 (2016) 2189–2198.
[19] G. He, J. Zhang, Y. Zhang, H. Chen, Fast and efficient removal of cationic dye using graphite oxide, adsorption, and kinetics studies, J. Disper. Sci. Technol., 34 (2013) 1223–1229.
[20] G.K. Ramesha, A.V. Kumara, H.B. Muralidhara, S. Sampath, Graphene and graphene oxide as effective adsorbents toward anionic and cationic dyes, J. Colloid. Interface Sci., 361 (2011) 270–277.
[21] B. Tryba, J. Przepiorski, A.W. Morawski, Influence of chemically prepared H_2SO_4-graphite intercalation compound (GIC) precursor on parameters of exfoliated graphite (EG) for oil sorption from water, Carbon, 41 (2002) 2009–2025.
[22] D.D.L. Chung, A review of exfoliated graphite, J. Mater. Sci., 51 (2016) 554–568.
[23] B. Tryba, A.W. Morawski, M. Inagaki, Preparation of exfoliated graphite by microwave irradiation, Carbon, 43 (2005) 2397–2429.
[24] T. Wei, Z. Fan, G. Luo, C. Zheng, D. Xie, A rapid and efficient method to prepare exfoliated graphite by microwave irradiation, Carbon, 47 (2008) 313–347.
[25] I. Do, L.T. Drzal, Ionic liquid-assisted synthesis of Pt nanoparticles onto exfoliated graphite nanoplatelets for fuel cells, ACS Appl. Mater. Interfaces., 6 (2014) 12126–12136.
[26] S.R. Dhakate, S. Sharma, M. Borah, R.B. Mathur, T.L. Dhami, Expanded graphite-based electrically conductive composites as bipolar plate for PEM fuel cell, Int. J. Hydrogen Energy, 33 (2008) 7146–7152.
[27] C. Santhosh, P. Kollu, S. Felix, V. Velmurugan, S.K. Jeong, A.N. Grace, $CoFe_2O_4$ and $NiFe_2O_4$@graphene adsorbents for heavy metal ions – kinetic and thermodynamic analysis, RSC Adv., 5 (2015) 28965–28972.
[28] S. Kittappa, S. Pichiah, J.R. Kim, Y. Yoon, S.A. Snyder, M. Jang, Magnetised nanocomposite mesoporous silica and its application for effective removal of methylene blue from aqueous solution, Sep. Purif. Technol., 153 (2015) 67–75.
[29] M.R. Lasheen, I.Y. El-Sherifb, M.E. Tawfik, S.T. El-Wakeel, M.F. El-Shahat, Preparation and adsorption properties of nano magnetite chitosan films for heavy metal ions from aqueous solution, Mater. Res. Bull., 80 (2016) 344–350.
[30] X. Fan, H. Gao, X. Kou, B. Zhang, S. Wang, Synthesis of FeCo-reduced graphene oxide composite and its magnetic and adsorption properties, Mater. Res. Bull., 65 (2015) 320–324.
[31] Y. Zhang, Z. Nan, Preparation of magnetic $ZnLa_{0.02}Fe_{1.98}O_4$/MWCNTs composites and investigation on its adsorption of methyl orange fromaqueous solution, Mater. Res. Bull., 66 (2015) 176–185.
[32] P. Lavela, J.L. Tirado, $CoFe_2O_4$ and $NiFe_2O_4$ synthesized by sol–gel procedures for their use as anode materials for Li ion batteries, J. Power Sources, 172 (2007) 379–387.
[33] V. Sepelak, I. Bergmann, A. Feldhoff, P. Heitjans, F. Krumeich, D. Menzel, F.J. Litterst, S.J. Campbell, K.D. Becker, Nanocrystalline Nickel Ferrite, $NiFe_2O_4$: mechanosynthesis, nonequilibrium cation distribution, canted spin arrangement, and magnetic behavior, J. Phys. Chem. C., 111 (2007) 5026–5033.
[34] M.E. Uddin, N.H. Kim, T. Kuila, S.H. Lee, D. Hui, J.H. Lee, Preparation of reduced graphene oxide-$NiFe_2O_4$ nanocomposites for the electrocatalytic oxidation of hydrazine, Composites Part B: Engineering, 79 (2015) 649–659.
[35] P.Y. Lee, K. Ishizaka, H. Suematsu, W. Jiang, K. Yatsui, Magnetic and gas sensing property of nanosized $NiFe_2O_4$ powders synthesized by pulsed wire discharge, J. Nanopart. Res., 8 (2006) 29–35.
[36] I. Khosravi, M. Eftekhar, Characterization and evaluation catalytic efficiency of $NiFe_2O_4$ nano spinel in removal of reactive dye from aqueous solution, Power Technol., 250 (2013) 147–153.
[37] E.L. Grabowska, G. Gryglewicz, Adsorption characteristics of Congo Red on coal-based mesoporous activated carbon, Dyes Pigm., 74 (2007) 34–40.
[38] Y. Umemur, E. Shinohara, R.A. Schoonhey, Preparation of Langmuir–Blodgett films of aligned sepiolite fibers and orientation of methylene blue molecules adsorbed on the film, Phys. Chem. Chem. Phys., 11 (2009) 9804–9810.
[39] X. Yua, C. Wei, H. Wu, Effect of molecular structure on the adsorption behavior of cationic dyes onto natural vermiculite, Sep. Purif. Technol., 156 (2015) 489–495.
[40] J.H. Huang, K.L. Huang, S.Q. Liu, A. Wang, C. Yan, Adsorption of rhodamine B and methyl orange on a hypercrosslinked polymeric adsorbent in aqueous solution, Colloids Surf. A., 330 (2008) 55–61.
[41] S. Chen, J. Zhang, C. Zhang, Q. Yue, Y. Li, C. Li, Equilibrium and kinetic studies of methyl orange and methyl violet adsorption on activated carbon derived from Phragmites australis, Desalination, 252 (2010) 149–156.
[42] K.Y. Foo, B.H. Hameed, Insights into the modeling of adsorption isotherm systems, Chem. Eng. J., 156 (2010) 2–10.
[43] X.V. Heerden, H. Badenhorst, The influence of three different intercalation techniques on the microstructure of exfoliated graphite, Carbon, 88 (2015) 173–184.
[44] V.S. Amar, J.A. Puszynski, R.V. Shende, H_2 generation from thermochemical water-splitting using yttria stabilized $NiFe_2O_4$ core-shell nanoparticles, J. Renew. Sustain. Ener., 7 (2015) 023113-1–023113-13.
[45] P. Li, R. Ma, Y. Zhou, Y. Chen, Q. Liu, G. Peng, Z. Liang, J. Wang Spinel nickel ferrite nanoparticles strongly cross-linked with multiwalled carbon nanotube as a Bi-efficient electrocatalyst for the oxygen reduction and oxygen evolution, RSC Adv., 5 (2015) 73834–73841.
[46] T. Suzuki, T. Okuhara, Change in pore structure of MFI zeolite by treatment with NaOH aqueous solution, Micropor. Mesopor. Mat., 43 (2001) 83–89.
[47] B.K. Nandi, A. Goswami, M.K. Purkait, Removal of cationic dyes from aqueous solutions by kaolin: Kinetic and equilibrium studies, Appl. Clay Sci., 42 (2009) 583–590.
[48] J. Shu, Z. Wang, Y. Huang, N. Huang, C. Ren, W. Zhang, Adsorption removal of congo red from aqueous solution by polyhedral Cu_2O nanoparticles: Kinetics, isotherms, thermodynamics and mechanism analysis, J. Alloy Compd., 633 (2015) 338–346.
[49] N.A. Travlou, G.Z. Kyzas, N.K. Lazaridis, E.A. Deliyanni, Graphite oxide/chitosan composite for reactive dye removal, Chem. Eng. J., 217 (2013) 256–265.
[50] G.K. Ramesha, A.V. Kumara, H.B. Muralidhara, S. Sampath, Fast dye removal from water by starch-based nanocomposites, J. Colloid. Interface Sci., 361 (2011) 270–277.
[51] J. Yu, Y. Le, B. Cheng, Fabrication and CO_2 adsorption performance of bimodal porous silica hollow spheres with amine-modified surfaces, RSC Adv., 2 (2012) 6784–6791.
[52] R.D. Waldron, Infrared Spectra of Ferrites, Phys. Rev., 99 (1955) 1727–1735.

[53] N.W. Grimes, A.J. Collett, Infrared adsorption spectra of ferrites, Nature-phys Sci., 230 (1971) 158.
[54] J.L. Ahlrichs, Hydroxyl stretching frequencies of synthetic Ni-, Al- and Mg- hydroxy interlayers in expanding clays, Clays Clay Miner., 16 (1968) 6–71.
[55] A. Ghaffar, M.N. Younis, Adsorption of organic chemicals on graphene coated biochars and its environmental implications, Green Process Synth., 3 (2014) 479–487.
[56] M. Doltabadi, H. Alidadi, M. Davoudi, Comparative study of cationic and anionic dye removal from aqueous solutions using sawdust-based adsorbent, Environ. Prog. Sustain Energy, 35 (2016) 1078–1090.
[57] D. Xu, Q. Xu, K. Wang, J. Chen, Z. Chen, Fabrication of free-standing hierarchical carbon nanofiber/graphene oxide/polyaniline films for supercapacitors, ACS Appl. Mater. Interfaces, 6 (2014) 200–209.
[58] E. Eren, Adsorption performance and mechanism in binding of azo dye by raw bentonite, CLEAN – Soil, Air, Water, 38 (2010) 758–763.
[59] M. Wawrzkiewicz, M. Wiśniewska, V.M. Gun'ko, V.I. Zarko, Adsorptive removal of acid, reactive and direct dyes from aqueous solutions and wastewater using mixed silica–alumina oxide, Power Technol., 278 (2015) 306–315.
[60] F. Cecen, O. Aktas, Activated carbon for water and wastewater treatment: Integration of adsorption and biological treatment: Wiley-VHC, 2011.
[61] X. Mao, C. Wang, X. Ma, M. Zhang, L. Liu, L. Zhang, L. Niu, Q. Zeng, Y. Yang, C. Wang, Molecular level studies on binding modes of labeling molecules with polyalanine peptides, Nanoscale, 3 (2011) 1592.